Acta Acustica 2022, **6**, 8

https://doi.org/10.1051/aacus/2022002

Available online at:
https://acta-acustica.edpsciences.org

SCIENTIFIC ARTICLE OPEN ACCESS

Characteristics and mechanism of coupling effects in parallel-cladded acoustic waveguides

Guanjun Yin[1,2], Pan Li[2], Xuebing Yang[2], Ye Tian[2], Jing Han[1,*], Wei Ren[1], and Jianzhong Guo[2,*]

[1] Key Laboratory of Modern Teaching Technology, Shaanxi Normal University, Xi'an 710062, China
[2] School of Physics and Information Technology, Shaanxi Normal University, Xi'an 710119, China

Received 8 October 2021, Accepted 5 January 2021

Abstract – The characteristics and mechanism of coupling effects between parallel cladded acoustic waveguides (PCAWs) are essential when considering their applications in acoustic wave control and signal processing. We investigated its characteristics and revealed the nature of the coupling effect using a theoretical model of two-dimensional PCAWs and simulation experiments. We derived the eigenmode equation describing the behavior of a single waveguide based on the wave acoustic theory and derived analytic expressions for the coupling effects in the PCAWs using the coupled mode theory. Using the finite-element method, we analyzed the waveguide coupling exhibited by this structure given different configurational and acoustic parameter settings. Both theoretical and simulated results indicate that the input wave directed into one of four ports of this structure propagates and tunnels alternately between the two waveguides. Our theoretical model established yields analytic relations between the coupling lengths as well as the dependence on parameters of the evanescent wave and the structure. Analyses indicate wave coupling in the two PCAWs is essentially mediated by the evanescent wave. The unique evolution of the acoustic wave in PCAWs can be employed to develop pure acoustic devices such as frequency-selective filters, directional couplers, and acoustic switches.

Keywords: Coupling effect, Cladded acoustic waveguide, Evanescent wave, Coupling length

1 Introduction

When a wave is inputted into one of four ports of a pair of parallel cladded waveguides, the wave propagates and tunnels alternately between the pair waveguides rather than being confined to propagate along the original incident waveguide. In the fields of optics, this coupling phenomenon is referred to as waveguide coupling [1–5]. Subsequent research focused on establishing an accurate theoretical model for both weak and strong waveguide coupling and revealed that the coupling is mediated by evanescent waves [5–10]. Optical waveguide coupling is widely employed in optical wave steering [11–14], pure optical switches [15, 16], directional couplers [17], and frequency-selective filters [18, 19]. The theoretical research and exploration of other applications of waveguide coupling in optics have continued unabated [20–22].

Similar to the coupling effect in optical waveguides, an analogous acoustic waveguide coupling effect is also widely applicable for acoustic wave control and signal processing. In 1994, coupled wave propagation in two guides through perforations was discussed theoretically by Kergomard and collaborators [23]. Later, in 2016, they analyzed the coupling between two waveguides consisting of periodic lattices of finite length in 2016 [24]. In 2005, Pennec and collaborators studied the resonant tunneling of acoustic waves in phononic crystal waveguides. Acoustic waves of a specific frequency (f) tunnel from one waveguide to another through a resonance cavity [25]. In the same year, Sun and colleagues analyzed the wave coupling between two parallel phononic crystal waveguides and evaluated the coupling length (CL) using numerical experiments [26]; here, CL is defined as the propagation distance necessary for an acoustic wave to transfer from an initial waveguide to an adjacent waveguide. In 2015, Maksimov and collaborators investigated the coupled-mode theory (CMT) of the acoustic resonance cavity [27]. In 2016, an acoustic add-drop filter was fabricated from two line-defect waveguides coupled through a resonator cavity based on a phononic crystal platform [28]. These studies focused mainly on the coupling between the phononic crystal waveguides and the resonance cavity.

Recently, the coupled waveguide network has been employed in the acoustic topological structure [29–31]. Shen and collaborators investigated super-mode propagation in a coupled waveguide complex [32] and demonstrated that with properly tailored couplings the sound was completely localized in one targeted intermediate cavity [33]. Molerón

*Corresponding authors: jhan2012@snnu.edu.cn; guojz@snnu.edu.cn

and collaborators investigated discrete propagation of trapped modes in airborne acoustic-waveguide arrays and showed the possibility of generating diffraction-free acoustic beams as well as focusing acoustic energy within a single lattice site [34]. However, little has been reported in studies of waveguide coupling in structures of cladded acoustic waveguides (CAWs) [35].

In 2018, we reported waveguide coupling in a CAW structure formed by two parallel ducts and realized acoustic focusing based on this effect in nested waveguides [36]. We found that when an acoustic wave is fed into one port of a waveguide of a pair of parallel ducts with fixed spacing, it propagates and tunnels back and forth between the ducts, with *CL* proportional to the wave frequency. In the same year, we studied the waveguide coupling in a structure of three parallel ducts and found that *CL* for two adjacent waveguides solely depends on the wave frequency and the spacing between the two cores but independent of the input mode [37]. Based on wave coupling in parallel waveguides, we can develop more acoustic devices analogs to those in optics. For example, tailoring the length of one waveguide of the structure equal to *CL* of a particular frequency, a pure acoustic device can be designed to realize frequency-selective filtering or even demodulating. The essential basis for those devices is the theoretical relationships between *CL* and the parameters such as wave frequency, core spacing, and material properties. The above studies demonstrated the phenomena and applications of waveguide coupling in the CAWs, but little is known of its mechanism and characteristics of the coupling effect from a theoretical point of view.

In this paper, we present a detailed theoretical model of waveguide coupling and reveal the mechanism and the characteristics of the coupling effects in two-dimensional parallel CAWs (PCAWs). First, we derive the analytic solutions of the eigenmode equation for a single CAW and reveal the propagation characteristics of an acoustic wave in both the cladding and core zones. Then, we derive the coupling equations for PCAWs and the parameter dependence of the coupling coefficients on both wave and structure using the CMT. Next, to verify theoretical results, the finite-element simulation is used to demonstrate and analyze waveguide coupling phenomena in the PCAWs for different core spacings and frequencies. The characteristics of evanescent waves in the cladding zone and the dependence of *CL* on core spacing and frequency are further compared and analyzed with the results. Finally, the characteristics of coupling effects are discussed and, its mechanism is revealed. The theoretical model may serve in applications of waveguide coupling to acoustic wave regulation and signal processing.

2 Theoretical model

2.1 Eigenmode equation in Single CAW

The structure of a single CAW is a core with cladding on both sides [35]. A cross-section of the two-dimensional model of the CAW (Fig. 1) was configured for the purpose

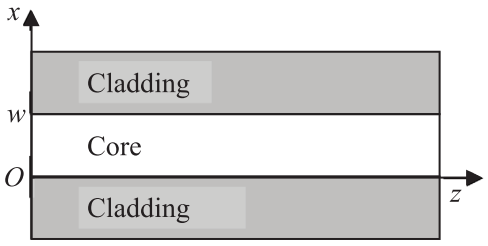

Figure 1. Schematic of a single CAW.

of simulations having a width w and density ρ_1 for the core zone, and a cladding density ρ_0. For the analysis, c_1, c_0, and c_a denote respectively the velocity of sound in the core, cladding, and air, respectively. The spatial distribution of the refractive index throughout the CAW may be written as

$$n(x,z) = \begin{cases} n_0 = \dfrac{c_a}{c_0}, & (x \le 0) \\ n_1 = \dfrac{c_a}{c_1}, & (0 \le x \le w) \\ n_0 = \dfrac{c_a}{c_0}, & (w \le x) \end{cases}. \tag{1}$$

Beginning with the equation governing the acoustic wave in two-dimensional free space,

$$\nabla^2_{x,z} p(x,z,t) - \frac{1}{c^2}\frac{\partial^2 p(x,z,t)}{\partial t^2} = 0, \tag{2}$$

where p denotes the acoustic pressure at position (x, z) at time t; we assume the solution of wave equation in the waveguide as

$$p(x,z,t) = \psi(x) e^{\mathrm{i}(\omega t - \beta z)}, \tag{3}$$

where $\psi(x)$ is the modal function of the wave in the waveguide, and $\omega = 2\pi f$ is the angular frequency. Substituting equation (3) into equation (2), we have

$$\left[\frac{\partial^2}{\partial x^2} + \left(k_a^2 n^2(x) - \beta^2\right)\right]\psi(x) = 0, \tag{4}$$

where k_a denotes the wave number of the wave in air. For a single CAW, the modal function is [4]

$$\psi(x) = \begin{cases} Ae^{qx}, & (x \le 0) \\ B\cos hx + C\sin hx, & (0 \le x \le w) \\ D(B\cos hw + C\sin hw)e^{-g(x-w)}, & (w \le x). \end{cases} \tag{5}$$

On substituting equation (5) into equation (4), we obtain

$$q = g = \sqrt{\beta^2 - \frac{\omega^2}{c_0^2}}, \tag{6}$$

$$h = \sqrt{\frac{\omega^2}{c_1^2} - \beta^2}. \tag{7}$$

Given that the sound pressure p and the vibration velocity v are continuous at $x = 0$ and $x = w$, we obtain the modal eigenvalue equation of the guided mode in a single CAW,

$$\tan hw = \frac{2\rho_0\rho_1 qh}{{\rho_0}^2h^2 - {\rho_1}^2q^2}. \tag{8}$$

Setting the normalized amplitude to unity ($A = 1$), the modal function of nth-order can be written as

$$\psi_n(x) = \begin{cases} e^{q_n x}, & (x \le 0) \\ \cos h_n x + \dfrac{q_n\rho_1}{h_n\rho_0}\sin h_n x, & (0 \le x \le w) \\ \left(\cos h_n w + \dfrac{q_n\rho_1}{h_n\rho_0}\sin h_n w\right)e^{-q_n(x-w)}, & (w \le x) \end{cases} \tag{9}$$

Equation (9) describes evanescent waves that strictly decay exponentially with penetration depth and q_n. The value of q_n depends on f and w in accordance with equations (6) and (8). Further analysis indicates that the evanescent wave also decays exponentially with f in a first approximation.

Moreover, from equations (6) to (8), the cut-off frequency for the nth-order mode is

$$f_{nc} = \frac{nc_1c_0}{2w\sqrt{c_0^2 - c_1^2}}. \tag{10}$$

As long as $f < f_{nc}$, the nth-order mode does not exist. That is, when f is less than f_{1c} of first-order mode, only one mode exists in the CAW regardless of the source condition.

2.2 Coupling equation for a PCAW

For the PCAW structure in two-dimensional cross-section (Fig. 2), we denote the densities of the cladding, core 1, and core 2 by ρ_0, ρ_1, and ρ_2, respectively; in addition, c_0, c_1, and c_2 denote the respective velocity of sound in these zones. The spatial distribution of the refraction index is written

$$n^2(x) = n_0^2 + \Delta n_l^2(x), \tag{11}$$

where $l = 1, 2$ denotes the core index; here, Δn_l^2 is only non-zero in the corresponding core.

To ensure that there is only one mode in the waveguides, a specific frequency range is chosen $f < f_{1c}$. In consequence, the expression for the wave front in the structure is expanded in the separable form,

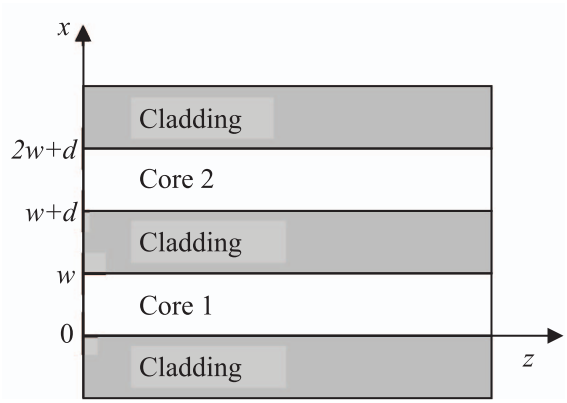

Figure 2. Cross-sectional schematic of the parallel cladded acoustic waveguide (PCAW) structure.

$$p = p_l(x)e^{-i\beta z} = \sum_{l=1}^{2}\psi_l(x)\xi_l(z)e^{-i\beta_l z}. \tag{12}$$

Substituting equation (12) into equation (2), we have

See the Equation (13) bottom of the page

Assuming that the wave amplitude of the coupled mode varies slowly with z, and combining with equation (4), equation (13) is simplified to

$$\begin{bmatrix} e^{-i\beta_1 z}\left(-\psi_1(x)2i\beta_1\dfrac{\partial\xi_1(z)}{\partial z} + \left(\dfrac{\omega^2}{c_2(x)^2} - \dfrac{\omega^2}{{c_0}^2}\right)\psi_1(x)\xi_1(z)\right) \\ +e^{-i\beta_2 z}\left(-\psi_2(x)2i\beta_2\dfrac{\partial\xi_2(z)}{\partial z} + \left(\dfrac{\omega^2}{c_1(x)^2} - \dfrac{\omega^2}{{c_0}^2}\right)\psi_2(x)\xi_2(z)\right) \end{bmatrix} = 0. \tag{14}$$

Multiplying both sides of equation (14) by $\psi_1(x)$ and $\psi_2(x)$ and integrating with respect to x while applying mode orthogonality, we obtain

$$\frac{\partial\xi_i(z)}{\partial z} = -i\kappa_{ii}\xi_i(z) - i\kappa_{ji}\xi_j(z)e^{-i(\beta_j - \beta_i)z} \tag{15}$$

where i, j represents number of the waveguide, $i, j = 1, 2$, and $i \ne j$. The coefficient of self-coupling is

$$\begin{bmatrix} \frac{\partial^2\psi_1(x)}{\partial x^2}\xi_1(z)e^{-i\beta_1 z} + \left(\frac{\omega^2}{{c_0}^2} + \left(\frac{\omega^2}{c_2(x)^2} - \frac{\omega^2}{{c_0}^2}\right) + \left(\frac{\omega^2}{c_1(x)^2} - \frac{\omega^2}{{c_0}^2}\right)\right)\psi_1(x)\xi_1(z)e^{-i\beta_1 z} \\ +\psi_1(x)\left(\frac{\partial^2\xi_1(z)}{\partial z^2} - 2i\beta_1\frac{\partial\xi_1(z)}{\partial z} - \beta_1^2\xi_1(z)\right)e^{-i\beta_1 z} \\ +\frac{\partial^2\psi_2(x)}{\partial x^2}\xi_2(z)e^{-i\beta_2 z} + \left(\frac{\omega^2}{{c_0}^2} + \left(\frac{\omega^2}{c_2(x)^2} - \frac{\omega^2}{{c_0}^2}\right) + \left(\frac{\omega^2}{c_1(x)^2} - \frac{\omega^2}{{c_0}^2}\right)\right)\psi_2(x)\xi_2(z)e^{-i\beta_2 z} \\ +\psi_2(x)\left(\frac{\partial^2\xi_2(z)}{\partial z^2} - 2i\beta_2\frac{\partial\xi_2(z)}{\partial z} - \beta_2^2\xi_2(z)\right)e^{-i\beta_2 z} \end{bmatrix} = 0 \tag{13}$$

$$\kappa_{ii} = \frac{\int_x k_0^2 \Delta n_j^2(x)\psi_i(x)\psi_i^*(x)\mathrm{d}x}{2\beta_i \int_x \psi_i(x)\psi_i^*(x)\mathrm{d}x} \tag{16}$$

and the coefficients of mutual-coupling is

$$\kappa_{ij} = \frac{\int_x k_0^2 \Delta n_j^2(x)\psi_i(x)\psi_j^*(x)\mathrm{d}x}{2\beta_j \int_x \psi_j(x)\psi_j^*(x)\mathrm{d}x}. \tag{17}$$

Here, we consider a symmetrical PCAW for which $\rho_1 = \rho_2$ and $c_1 = c_2$. Then, by calculating the integrals of equations (16) and (17) directly, we obtain

See the Equations (18) and (19) bottom of the page

Given initial conditions $\xi_1(0) = 1$ and $\xi_2(0) = 0$, the analytical solutions of equation (15) is

$$\xi_1(z) = \frac{1}{2}\left(e^{-i(\kappa+K)z} + e^{i(\kappa-K)z}\right), \tag{20a}$$

$$\xi_2(z) = \frac{1}{2}\left(e^{-\mathrm{i}(\kappa+K)z} - e^{\mathrm{i}(\kappa-K)z}\right). \tag{20b}$$

In view of equations (18) and (19), K is much smaller than κ and has no theoretical dependence on CL. We therefore omit it in equations (20a) and (20b) and hence obtain for the variation in acoustic power of the two waveguides,

$$P_1(z) = \cos^2(\kappa z), \tag{21a}$$

$$P_2(z) = \sin^2(\kappa z). \tag{21b}$$

Therefore, CL, defined as the propagation distance necessary to realize the maximum power transfer from an initial waveguide to an adjacent waveguide, is

$$CL = \frac{\pi}{2\kappa}. \tag{22}$$

3 Theoretical analyses and simulations of PCAW coupling

To verify the theoretical model and investigate the coupling effects systematically, we studied the series of scenarios for a structure with fixed configurational settings of $w = 2$ mm, $\rho_0 = 2700$ kg/m^3, $c_0 = 6260$ m/s, $\rho_1 = 998$ kg/m^3, and $c_1 = 1480$ m/s. The frequency varies from 200 to 350 kHz, and the core spacing varies from $d = 1.4$ mm to 2.2 mm.

3.1 Theoretical analyses

Using equations (8), (18), and (19), the values of κ and K were calculated (Tab. 1).

The results confirm the prediction that K is much smaller than κ by about three orders of magnitude, which is the assumption imposed in obtaining equations (21a) and (21b). Moreover, using equation (22) and the κ values listed (Tab. 1), theoretical values of CL for specific f and d were determined (Tab. 2).

3.2 Simulation experiments

Using the finite-element method, we conducted a series of simulations to evaluate wave coupling appearing in various PCAW structures. The configuration and parameter settings were the same as those in the theoretical studies. The amplitude of the acoustic wave was fixed at $P_A = 10^5$ Pa.

In snapshots of the acoustic wave propagating in the PCAW structure for various f and fixed d, we plotted the effective intensity distribution I_e (Fig. 3a) and the corresponding curves along the central axis of the input waveguide (Fig. 3b).

In a similar analysis, we simulated acoustic waves with fixed f propagating in PACW structure of distinct d. We plotted the distribution of I_e (Fig. 4a) and the corresponding effective intensity curves along the central axis of the input waveguide (Fig. 4b).

Rather than being confined to the input waveguide, the wave alternates periodically between the two waveguides along the propagation direction with a fixed period (Figs. 3a and 4a). The intensity distributions and curves indicate clearly that CL is proportional to f and d. Moreover, by analyzing the intensity curves along the input waveguide obtained from a series of simulations, we evaluated CL for different f and d (Tab. 3).

4 Analyses and discussion

4.1 Characteristics of wave coupling in the PCAW structure

To compare theoretical and simulation results, we plotted the CL values of Tables 2 and 3 (Fig. 5). The coupling length CL increases approximately exponentially for both

$$K = \kappa_{11} = \kappa_{22} = \frac{e^{-2q(w+d)}(e^{2qw}-1)(h^3\rho_0 - hq^2(\rho_0 - 2\rho_1))^2}{2\beta\left(2(h^2\rho_0 + q^2\rho_1)^2 + qw(h^2+q^2)(h^2\rho_0^2 + q^2\rho_1^2)\right)}, \tag{18}$$

$$\kappa = \kappa_{21} = \kappa_{12} = \frac{e^{-q(w+d)}h^2q^2\rho_0\left((h^2+q^2)(\rho_1-\rho_0) - e^{qw}(q^2(\rho_0-3\rho_1) + h^2(\rho_1-3\rho_0))\right)}{\beta\left(2(h^2\rho_0 + q^2\rho_1)^2 + qw(h^2+q^2)(h^2\rho_0^2 + q^2\rho_1^2)\right)}. \tag{19}$$

Table 1. Coefficients of self- and mutual- coupling obtained from analytical expressions.

d (mm)		f (kHz)						
		200	225	250	275	300	325	350
1.4	κ (m^{-1})	53.63	45.20	37.75	31.33	25.89	21.33	17.53
	K (10^{-3} m^{-1})	496.41	208.34	78.46	24.61	5.22	0.234	0.48
1.6	κ (m^{-1})	46.89	38.71	31.67	25.75	20.84	16.81	13.53
	K (10^{-3} m^{-1})	379.41	152.82	55.22	16.62	3.38	0.15	0.28
1.8	κ (m^{-1})	40.99	33.15	26.57	21.16	16.77	13.25	10.45
	K (10^{-3} m^{-1})	289.99	112.09	38.86	11.22	2.19	0.09	0.17
2.0	κ (m^{-1})	35.84	28.39	22.29	17.39	13.50	10.45	8.06
	K (10^{-3} m^{-1})	221.64	82.22	27.35	7.58	1.42	0.06	0.10
2.2	κ (m^{-1})	31.33	24.32	18.70	14.29	10.86	8.23	6.23
	K (10^{-3} m^{-1})	169.40	60.30	19.25	5.12	0.92	0.03	0.06

Table 2. Coupling lengths obtained from theoretical model (mm).

d (mm)	f (kHz)						
	200	225	250	275	300	325	350
1.4	29.29	34.75	41.61	50.13	60.67	73.66	89.62
1.6	33.50	42.76	49.60	61.01	75.38	93.44	116.09
1.8	38.32	47.38	59.12	74.24	93.66	118.54	150.37
2.0	43.83	55.32	70.47	90.35	116.37	150.38	194.77
2.2	50.14	64.59	84.00	109.95	144.59	190.77	252.29

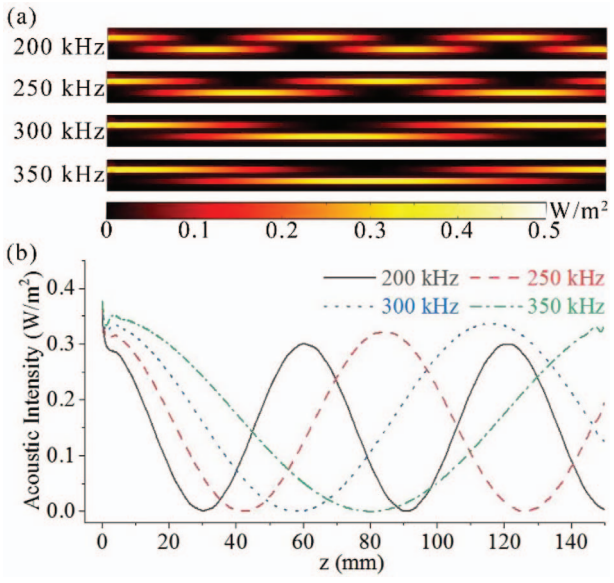

Figure 3. Simulated results of wave coupling in the PCAW structure for various f and fixed d = 1.4 mm: (a) acoustic intensity distribution, (b) acoustic intensity curves along the central-axis of the input waveguide.

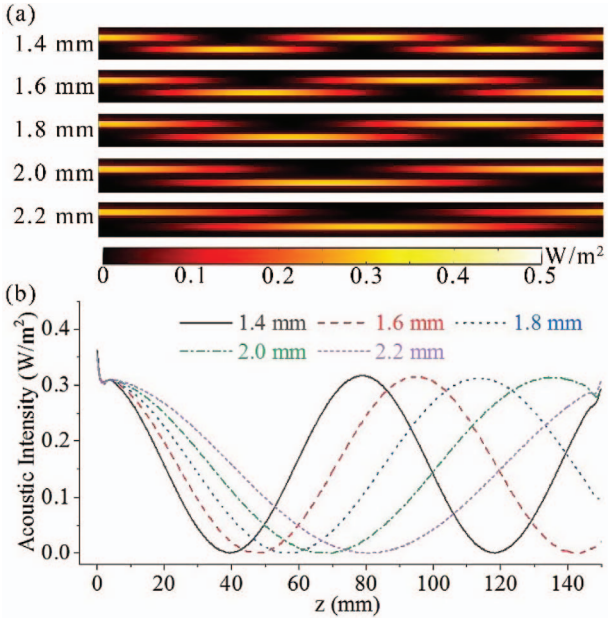

Figure 4. Simulated results of wave coupling in the PCAW structures for various d and fixed frequency f = 240 kHz: (a) acoustic intensity distribution, (b) acoustic intensity curves along the central-axis of the input waveguide.

Table 3. Values of the coupling length CL (mm) obtained from the simulations.

d (mm)	f (kHz)						
	200	225	250	275	300	325	350
1.4	30.23	35.79	42.14	49.42	58.00	68.04	80.00
1.6	35.69	42.70	50.92	60.65	72.64	86.72	104.01
1.8	41.47	50.45	61.16	74.39	90.71	110.60	135.02
2.0	48.51	59.57	73.65	91.22	113.03	140.42	175.14
2.2	56.05	70.24	88.38	110.70	140.69	178.58	227.18

f and d in accordance with the dependence of the evanescent wave on f and d. Furthermore, discrepancies in the plot are evident between the theoretical and simulation results. Therefore, we analyzed the relative error in CL between these results (Tab. 4).

Viewing Table 4, the max error is 12.03% and the average error is 5.66%. The smallest error is 0.20% and most errors are smaller than 10.00%. Neglecting the quadratic terms in equation (13) and the accuracy of the modal eigenvalues for a single CAW, we found that both contribute to

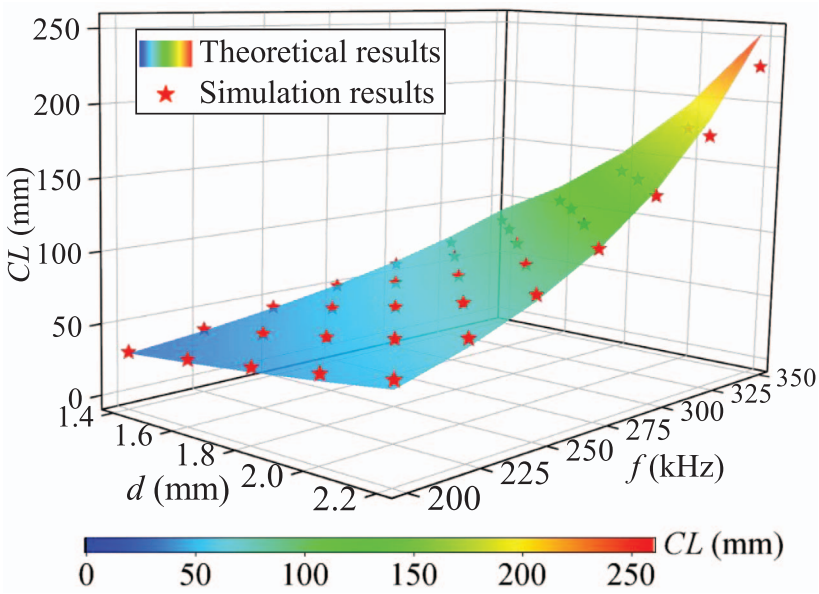

Figure 5. *CL* values obtained from theory (colored surface) and simulation (red stars).

Table 4. Relative errors between *CL* from the theoretical and simulated results (%).

d (mm)	f (kHz)						
	200	225	250	275	300	325	350
1.4	−3.11	−2.90	−1.26	1.44	4.60	8.25	12.03
1.6	−6.13	−4.97	−2.60	0.59	3.77	7.75	11.61
1.8	−7.59	−6.09	−3.34	−0.20	3.25	7.18	11.37
2.0	−9.64	−7.14	−4.32	−0.94	2.96	7.09	11.21
2.2	−10.55	−8.04	−4.96	−0.67	2.77	6.83	11.05

those errors. Indeed, in conducting more analysis on an input wave of $f = 375$ kHz, the errors become even larger. The reason is that the wave frequency exceeds the cut-off frequency for the first-order mode and the wave propagate along the waveguide as two modes, a scenario that is not considered in our theoretical analysis. Nevertheless, the theoretical model presented helps to reveal the nature of the wave coupling in the PCAW structures and predicts *CL* values for a single mode accurately.

4.2 Nature of wave coupling in a PCAW structure

Both coefficients of self- and mutual-coupling, equations (16) and (17), were determined using the overlap integrals of the guide modes and calculated by integral segmentation. Because Δn_i^2 is non-zero only in this part of the core, the integration for κ_{11} is non-zero in this section of core 2 and depends on the evanescent wave of waveguide 1. Analogously, κ_{22} depends on the evanescent wave of waveguide 2, κ_{12} on the evanescent wave of waveguide 1 and the guided wave of waveguide 2, and κ_{21} on the evanescent wave of waveguide 2 and the guided wave of waveguide 1. For symmetrical parallel waveguides, K describes the leakage of the evanescent wave and κ describes the interaction between the evanescent wave of one waveguide and the guided wave in the adjacent waveguide.

The evanescent wave decays exponentially with penetration depth and with f in an approximate exponential form; similarly, κ (CL) decays (increases) with d in strict exponential form and with f in an approximate exponential form. Considering the above analyses, we are assured that the coupling effect in a PCAW structure is essentially an evanescent wave coupling. When the evanescent wave is weaker, the wave coupling is weaker; for a complete wave coupling process, *CL* is longer. Enlarging the wave frequency, widening the spacing between cores, and, of course, increasing the material difference between the cladding and core weakens the evanescent wave and certainly suppresses waveguide coupling.

5. Conclusions

Applying the wave acoustic theory, we presented the propagation characteristics of acoustic waves in both the cladding and core zones of a single CAW by imposing appropriate continuous boundary conditions. A theoretical model of wave coupling in a pair of PCAWs was established by combining the modal functions of the single waveguide and CMT.

Both the nature and characteristics of the wave coupling were analyzed based on results obtained from theoretical modal and simulations. The analysis revealed that: (1) evanescent waves exist in the cladding zone of the single CAW and decrease exponentially with increasing d and f, the latter only approximately; (2) *CL* increases exponentially with increasing d and f approximately; (3) and from those two observations, we concluded that as d and f

increased, the evanescent wave became weaker, resulting in a longer propagation distance (*CL*) required for the acoustic wave to transfer from one waveguide to the adjacent waveguide. Thus, the acoustic wave coupling in the two waveguides is mediated by the evanescent wave in the cladding. In theory, the coupling process does not break down. Circumstances may weaken the coupling and increase the *CL*. When the structure length is much smaller than *CL*, the coupling process is incomplete and weak, and it could be barely observed.

Our results regarding the waveguide coupling support their further application in the field of acoustic wave control and signal processing. Potentially, pure acoustic devices such as frequency selectors, focusing devices, and coupling switches may be designed given appropriate settings of the *CL* characteristics.

Acknowledgments

This work was supported by the National Natural Science Foundation of China (Grant No. 12004237, 11727813, 12034005 and 12174004), the China Postdoctoral Science Foundation (Grant No. 2020M683416), the Fundamental Research Funds for the Central Universities (Grant No. GK202003090), and the Key Laboratory of Ultrasound of Shaanxi Province, China.

References

1. E.A.J. Marcatili: Dielectric rectangular waveguide and directional coupler for integrated optics. Bell System Technical Journal 48 (1969) 2071–2102.
2. D. Marcuse: The coupling of degenerate modes in two parallel dielectric waveguides. Bell System Technical Journal 50 (1971) 1791–1816.
3. A.W. Snyder: Coupled-mode theory for optical fibers. Journal of the Optical Society of America 62 (1972) 1267–1277.
4. A. Yariv: Coupled-mode theory for guided-wave optics. IEEE Journal of Quantum Electronics 9 (1973) 919–933.
5. W.P. Huang: Coupled-mode theory for optical waveguides: an overview. Journal of the Optical Society of America A 11 (1994) 963–983.
6. A. Hardy, S. Shakir, W. Streifer: Coupled-mode equations for two weakly guiding single-mode fibers. Optics Letters 11 (1986) 324–326.
7. A. Hardy, W. Streifer: Coupled mode solutions of multiwaveguide systems. IEEE Journal of Quantum Electronics 22 (1986) 528–534.
8. A.W. Snyder, A. Ankiewicz, A. Altintas: Fundamental error of recent coupled mode formulations. Electronics Letters 20 (1987) 1097–1098.
9. A. Hardy, W. Streifer, M. Osinski: Weak coupling of parallel waveguides. Optics Letters 13 (1988) 161–163.
10. K. Yasumoto: Coupled-mode formulation of parallel dielectric waveguides. Optics Letters 18 (1993) 503–504.
11. M.F. Yanik, S. Fan: Stopping and storing light coherently. Physical Review A 71 (2005) 013803.
12. L. Verslegers, P.B. Catrysse, Z. Yu, S. Fan: Deep-subwavelength focusing and steering of light in an aperiodic metallic waveguide array. Physical Review Letters 103 (2009) 033902.
13. I. Biaggio, V. Coda, G. Montemezzani: Coupling-length phase matching for nonlinear optical frequency conversion in parallel waveguides. Physical Review A 90 (2014) 043816.
14. H. Leblond, S. Terniche: Waveguide coupling in the few-cycle regime. Physical Review A 93 (2016) 043839.
15. S.R. Friberg, P.W. Smith: Nonlinear optical glasses for ultrafast optical switches. IEEE Journal of Quantum Electronics 23 (1987) 2089–2094.
16. K.S. Chiang: Coupled-mode equations for pulse switching in parallel waveguides. IEEE Journal of Quantum Electronics 33 (1997) 950–954.
17. H. Kogelnik, R.V. Schmidt: Switched directional couplers with alternating $\Delta\beta$. IEEE Journal of Quantum Electronics 12 (1976) 396–401.
18. R.C. Alferness, P. Cross: Filter characteristics of codirectionally coupled waveguides with weighted coupling. IEEE Journal of Quantum Electronics 14 (1978) 843–847.
19. M. Qiu, M. Mulot, M. Swillo, S. Anand, B. Jaskorzynska, A. Karlsson: Photonic crystal optical filter based on contradirectional waveguide coupling. Applied Physics Letters 83 (2003) 5121–5123.
20. P. Paddon, J.F. Young: Two-dimensional vector-coupled-mode theory for textured planar waveguides. Physical Review B 61 (2000) 2090.
21. Z. Gao, D. Siriani, K.D. Choquette: Coupling coefficient in antiguided coupling: magnitude and sign control. Journal of the Optical Society of America B 35 (2018) 417–422.
22. G. Bellanca, P. Orlandi, P. Bassi: Assessment of the orthogonal and non-orthogonal coupled-mode theory for parallel optical waveguide couplers. Journal of the Optical Society of America A 35 (2018) 577–585.
23. J. Kergomard, A. Khettabi, X. Mouton: Propagation of acoustic waves in two waveguides couples by perforations. I. Theory. Acta Acustica 2 (1994) 1–16.
24. M. Pachebat, J. Kergomard: Propagation of acoustic waves in two waveguides coupled by perforations. II. Analysis of periodic lattices of finite length. Acta Acustica united with Acustica 102 (2016) 611–625.
25. Y. Pennec, B. Djafari-Rouhani, J.O. Vasseur, H. Larabi: Acoustic channel drop tunneling in a phononic crystal. Applied Physics Letters 87 (2005).
26. J.H. Sun, T.T. Wu: Analyses of mode coupling in joined parallel phononic crystal waveguides. Physical Review B 71 (2005).
27. D.N. Maksimov, A.F. Sadreev, A.A. Lyapina, A.S. Pilipchuk: Coupled mode theory for acoustic resonators. Wave Motion 56 (2015) 52–66.
28. B. Rostami-Dogolsara, M.K. Moravvej-Farshi, F. Nazari: Acoustic add-drop filters based on phononic crystal ring resonators. Physical Review B 93 (2016) 014304.
29. M. Molerón, G. Dubois, O. Richoux, S. Félix, V. Pagneux: Reduced modal modelling of time-domain propagation in complex waveguide networks. Acta Acustica united with Acustica 100 (2014) 391–400.
30. Q. Wei, Y. Tian, S.Y. Zuo, Y. Cheng, X.J. Liu: Experimental demonstration of topologically protected efficient sound propagation in an acoustic waveguide network. Physical Review B 95 (2017) 094305.
31. Y.G. Peng, Z.G. Geng, X.F. Zhu: Topologically protected bound states in one-dimensional Floquet acoustic waveguide systems. Journal of Applied Physics 123 (2018) 091716.
32. Y.X. Shen, Y.G. Peng, X.C. Chen, D.G. Zhao, X.F. Zhu: Observation of low-loss broadband supermode propagation in coupled acoustic waveguide complex. Scientific Reports 7 (2017) 45603.

33. Y.X. Shen, Y.G. Peng, D.G. Zhao, X.C. Chen, J. Zhu, X.F. Zhu: One-way localized adiabatic passage in an acoustic system. Physical Review Letters 122 (2019) 094501.
34. M. Moleron, C. Faure, S. Felix, V. Pagneux, O. Richoux: Discrete propagation of trapped modes in acoustic waveguide arrays. Physical Review B 99 (2019) 201404.
35. G.D. Boyd, L.A. Coldren, R.N. Thurston: Acoustic waveguide with a cladded core geometry. Applied Physics Letters 26 (1975) 31.
36. G.J. Yin, T. Zhang, W. Wang, Y.H. Xin, J.Z. Guo: Focusing phenomenon based on the coupling effect of acoustic waveguide. Ultrasonics 84 (2018) 9–12.
37. G.J. Yin, P. Li, J.Z. Guo, S.Y. Lin, H. Cao: Coupling Effects in Three Parallel Waveguides. 2018 IEEE International Ultrasonics Symposium, Kobe, Japan, October 22–25 (2018) pp. 1–9.

Cite this article as: Yin G. Li P. Yang X. Tian Y. Han J, et al.. 2022. Characteristics and mechanism of coupling effects in parallel-cladded acoustic waveguides. Acta Acustica, **6**, 8.